Parallel Metallocenes of Germanium, Tin, and Lead

Steven P. Constantine, Hazel Cox, Peter B. Hitchcock, and Gerard A. Lawless*

The Chemistry Laboratory, School of Chemistry, Physics and Environmental Science, University of Sussex, Brighton, U.K. BN1 9QJ

Received November 2, 1999

The reaction of 2 equiv of $LiCp^s$ ($Cp^s = C_5Me_4(SiMe_2Bu^t)$) with $GeCl_2$·diox, $SnCl_2$, or $PbCl_2$ in ethereal solvents affords the metallocenes $[M(\eta^5\text{-}Cp^s)_2]$ (M = Ge, **1**; M = Sn, **2**; M = Pb, **3**) in 96, 89, and 84% yields, respectively. A single-crystal X-ray structural analysis of each reveals that, for the first time, the cyclopentadienyl rings are parallel for all three metallocenes. Both solid- and solution-state multinuclear NMR spectroscopic data for **2** and **3** are reported. An examination of **1**−**3** using DFT has also been performed, and in the case of **1** a comparison with its C_5H_5 analogue has been carried out.

Introduction

Sterically demanding, cyclopentadienyl-based ligands have played an important role in organometallic chemistry for almost four decades. Primarily, such ligands serve to prevent the oligomerization or polymerization of electronically and coordinatively unsaturated species. Secondarily, however, such ligands serve to impart kinetic stabilization to otherwise highly reactive species, notably so when the metal center is a main-group element.[1] Furthermore, when they are applied to early transition metals and lanthanides, these ligands have led to an impressive range of catalysts. It is possible to control both the steric saturation about the metal center, which influences the selectivity of the catalyst, and also the Lewis acidity at the metal center by varying the cyclopentadienyl substituents.[2] With these features in mind, we have turned our attention to the synthesis of a mixed alkyl- and silyl-substituted cyclopentadienyl system, $^-Cp^s$ ($Cp^s = C_5Me_4(SiMe_2Bu^t)$). The steric and electronic properties of this unique cyclopentadienyl ligand have enabled the structural characterization of three parallel group 14 metallocenes $[M(\eta^5\text{-}Cp^s)_2]$ (M = Ge, **1**; M = Sn, **2**; M = Pb, **3**). Prior to our communications of the structural characterization of **2**[3] and **3**[4] only two parallel metallocenes of the group 14 elements had been structurally characterized, i.e. $[Sn(\eta^5\text{-}C_5Ph_5)_2]$[5] and $[Si(\eta^5\text{-}C_5Me_5)_2]$.[6] Isomorphism for the Ge and Pb analogues of the former was not established, though it was inferred from X-ray powder diffraction data. Since then two further parallel metallocenes of Sn[7] and Pb,[8] containing pentaisopropyl- and triisopropylcyclopentadienyl ligands, respectively, have appeared. As the existence of parallel metallocenes of C has been ruled out on the basis of theoretical studies,[9] Ge remains the only group 14 element for which a parallel metallocene has not been structurally characterized. This absence has been attributed to both steric and electronic factors: i.e., ring slippage to relieve steric congestion at the Ge center when bulky ligands are employed and more facile s−p mixing for Ge in comparison to Sn and Pb. However, to date all theoretical studies have shown that the parallel form of $Ge(\eta^5\text{-}C_5H_5)_2$ is more stable than its bent isomer. Thus, as an extension to our previous communications we now report the synthesis and molecular structure of the first parallel germanocene derivative, $[Ge(\eta^5\text{-}Cp^s)_2]$, and along with its Sn and Pb analogues offer an examination of the molecular orbital energies of this unique series of metallocenes using density functional theory (DFT).

Scheme 1

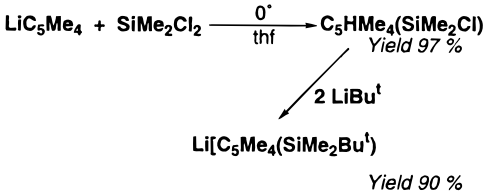

Results and Discussion

The lithium reagent $LiCp^s$ was synthesized in two stages, commencing with the preparation of $C_5HMe_4(SiMe_2Cl)$ by the reaction of LiC_5HMe_4 and $SiMe_2Cl_2$ followed by the one-pot alkylation at Si and metalation of the cyclopentadienyl ring, by 2 equiv of $LiBu^t$. Compounds **1**−**3** were prepared by the reaction of 2 equiv of $LiCp^s$ with $GeCl_2$·diox (diox = dioxane), $SnCl_2$, and $PbCl_2$ in ethereal solvents, affording the metallocenes in 96, 89, and 84% yields, respectively (Scheme 1). Recrystallization from either hot toluene, in the case of **1**, or hexanes for **2** and **3** afforded crystalline solids.

The molecular structures of **1**−**3** were determined (Table 1) and revealed that in each case the metal atom

(1) Jutzi, P.; Burford, N. D. *Chem. Rev.* **1999**, *99*, 969 and references therein.
(2) See e.g.: Togni, A.; Halterman, R. L. *Metallocenes*; Wiley-VCH: Weinheim, Germany, 1998.
(3) Constantine, S. P.; Hitchcock, P. B.; Lawless, G. A.; de Lima, G. M. *J. Chem. Soc., Chem. Commun.* **1996**, 1101.
(4) Constantine, S. P.; Hitchcock, P. B.; Lawless, G. A. *Organometallics* **1996**, *15*, 3905.
(5) Heeg, M. J.; Janiak, C.; Zuckerman, J. J. *J. Am. Chem. Soc.* **1984**, *106*, 4259.
(6) Jutzi, P.; Kanne, D.; Krüger, C. J. *Angew. Chem., Int. Ed. Engl.* **1985**, *24*, 773 (the unit cell also contains a second bent isomer).
(7) Sitzmann, H.; Boese, R.; Stellberg, P. *Z. Anorg. Allg. Chem.* **1996**, *622*, 751−755.
(8) Hays, M. L.; Hanusa, T. P. *Adv. Organomet. Chem.* **1996**, *40*, 117.
(9) Schoeller, W. W.; Friedrich, O.; Sundermann, A.; Rozhenko, A. *Organometallics* **1999**, *18*, 2099.

10.1021/om990884z CCC: $19.00
Publication on Web 01/04/2000

Table 1. Structure Determination Summary for 1−3[a]

	1	2	3
	Crystal Data		
empirical formula	$C_{30}H_{54}Si_2Ge$	$C_{30}H_{54}Si_2Sn$	$C_{30}H_{54}Si_2Pb$
M_r	543.5	589.6	678.1
temp/K	293(2)	293(2)	173(2)
color, habit	pale yellow needles	yellow needles	red needles
unit cell dimens			
a/Å	13.207(4)	13.126(2)	12.945(3)
b/Å	8.781(4)	9.135(7)	9.219(4)
c/Å	13.844(3)	13.769(2)	13.661(4)
α/deg	90	90	90
β/deg	92.25(2)	92.41(10)	93.96(2)
γ/deg	90	90	90
V/Å^3	1604.3(9)	1649.5(13)	1626.4(9)
D_{calcd}/Mg m^{-3}	1.13	1.19	1.39
μ/mm^{-1}	1.05	0.86	5.28
F(000)	588	624	688
	Data Collection		
2*θ* range/deg	2.0−30	2.0−25.0	2.0−28.0
index ranges, *hkl*	0−18, 0−12, −19 to +19	0−15, 0−10, −16 to +16	0−17, 0−12, −18 to +17
no. of rflns collected	4835	3019	4059
no. of indep rflns	4662 (R_{int} = 0.0590)	2892 (R_{int} = 0.0182)	3903 (R_{int} = 0.0271)
no. of obsd rflns ($I > 2\sigma(I)$)	1949	1956	2734
structure soln	isomorphous with **2**	direct methods	isomorphous with **2**
no. of params refined	155	155	156
R1 (obsd data), wR2 (all data)	0.084, 0.207	0.043, 0.092	0.044, 0.104
goodness of fit on F^2	1.036	1.067	1.221

[a] Details in common: crystal size 0.3 × 0.3 × 0.2 mm; monoclinic, space group $P2_1/n$ (nonstandard No. 14); $Z = 2$, Enraf-Nonius CAD4 diffractometer, Mo Kα radiation (λ = 0.710 73 Å). H atoms were included in the riding mode with $U_{iso}(H) = 1.5[U_{eq}(C)]$.

was positioned between equidistant cyclopentadienyl rings which were planar, staggered, and exactly parallel. The silyl substituents of the Cp^s rings were *trans* to one another, with the silyl−Me groups directed toward, and the Bu^t groups away from, the metal centers. The C(1)−Si bond was bent out of the plane of the Cp^s rings and away from the metal centers by 4.1 and 1.8° for **1** and **2**, respectively, but was coplanar with the Cp^s rings for **3** (Figure 1). This bend thus reflects the increased inter-ring steric repulsions arising from the decreasing covalent radii of the metal centers. The centroid−metal distances (2.211(5), 2.379(2), and 2.460(5) Å for **1**−**3**, respectively (Tables 2 and 3)) represent the shortest metal−centroid distances measured to date for any of their respective metallocene analogues. Indeed, in each case the metal−cyclopentadienyl-centroid distances are shorter than those observed for their C_5H_5 analogues (Tables 4−6). The proximity with which the Cp^s ligand can approach the metal centers results in an increase in the steric demands of this ligand when compared with those of other cyclopentadienyl ligands of similar or increased bulk. These steric constraints are augmented by the presence of the Bu^t substituents which, due to hindered rotation about the C(1)−Si bond, remain perpendicular to the plane of the cyclopentadienyl ring and direct both silyl Me groups toward the metal centers, resulting in 12 Me groups directed toward the plane containing the metal centers. When the Bu^t substituents are replaced by Me groups, as in the case of [Sn{$C_5Me_4(SiMe_3)$}$_2$] and [Pb{$C_5Me_4(SiMe_3)$}$_2$], rotation about the C(1)−Si bond occurs and both molecular structures display nonparallel rings.[10]

Density Functional Theory Treatment of 1−3. An examination of **1**−**3** by DFT with a view to elucidating the nature of the bonding in this novel series of parallel metallocenes was performed. Prior to presenting

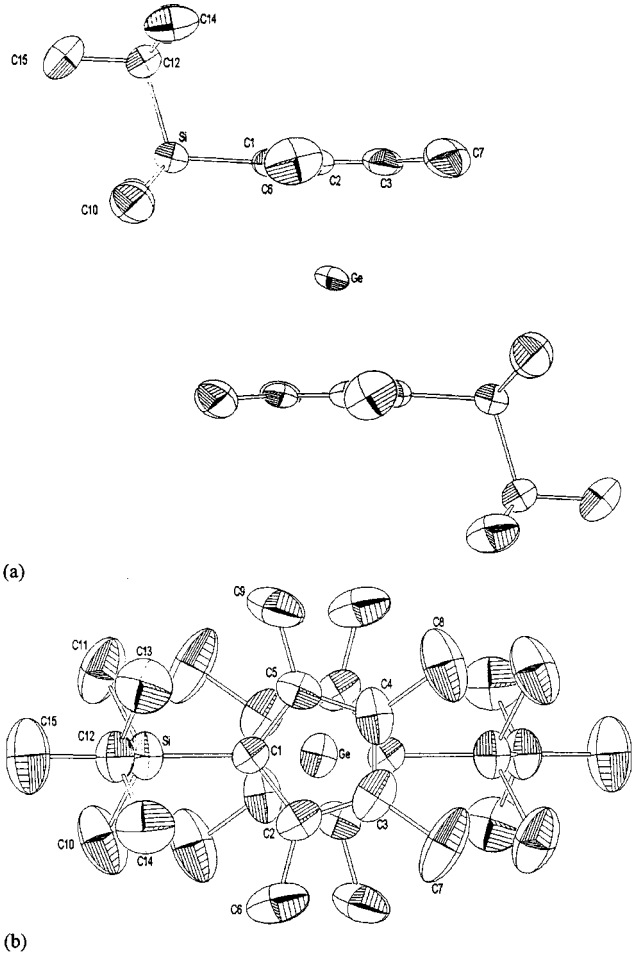

Figure 1. (a) Profile and (b) top ORTEP views of **1**, showing the atom-labeling scheme. The thermal ellipsoids are drawn at the 50% probability level.

the MO diagram of **1**−**3**, it is instructive to examine the effect of the silyl substituent on the frontier orbitals of

(10) Keates, J. M. Ph.D. Thesis, University of Sussex, 1997.

Table 2. Selected Bond Lengths (Å) for 1−3

1				2				3			
Ge−M(1)[a]	2.211(5)	C(1)−C(5)	1.419(6)	Sn−M(1)	2.379(2)	C(1)−C(5)	1.426(6)	Pb−M(1)	2.460(5)	C(1)−C(5)	1.430(7)
Ge−C(1)	2.499(4)	C(2)−C(3)	1.405(7)	Sn−C(1)	2.637(4)	C(2)−C(3)	1.402(6)	Pb−C(1)	2.707(5)	C(2)−C(3)	1.408(7)
Ge−C(2)	2.511(5)	C(2)−C(6)	1.494(7)	Sn−C(2)	2.652(4)	C(2)−C(6)	1.512(7)	Pb−C(2)	2.731(5)	C(2)−C(6)	1.503(8)
Ge−C(3)	2.521(5)	C(3)−C(4)	1.389(7)	Sn−C(3)	2.685(5)	C(3)−C(4)	1.403(7)	Pb−C(3)	2.770(5)	C(3)−C(4)	1.438(8)
Ge−C(4)	2.529(5)	C(3)−C(7)	1.503(7)	Sn−C(4)	2.691(5)	C(3)−C(7)	1.504(7)	Pb−C(4)	2.773(5)	C(3)−C(7)	1.495(8)
Ge−C(5)	2.509(4)	C(4)−C(5)	1.405(7)	Sn−C(5)	2.661(4)	C(4)−C(5)	1.410(6)	Pb−C(5)	2.736(5)	C(4)−C(5)	1.413(7)
Si−C(1)	1.868(5)	C(4)−C(8)	1.518(8)	Si−C(1)	1.872(4)	C(4)−C(8)	1.501(7)	Si−C(1)	1.869(5)	C(4)−C(8)	1.505(8)
Si−C(10)	1.860(6)	C(5)−C(9)	1.501(7)	Si−C(10)	1.873(6)	C(5)−C(9)	1.501(6)	Si−C(10)	1.874(6)	C(5)−C(9)	1.514(7)
Si−C(11)	1.872(6)	C(12)−C(13)	1.515(8)	Si−C(11)	1.872(5)	C(12)−C(13)	1.526(7)	Si−C(11)	1.866(6)	C(12)−C(13)	1.528(8)
Si−C(12)	1.899(5)	C(12)−C(14)	1.521(8)	Si−C(12)	1.894(5)	C(12)−C(14)	1.542(7)	Si−C(12)	1.899(6)	C(12)−C(14)	1.539(8)
C(1)−C(2)	1.419(6)	C(12)−C(15)	1.547(7)	C(1)−C(2)	1.423(6)	C(12)−C(15)	1.544(7)	C(1)−C(2)	1.444(7)	C(12)−C(15)	1.538(8)

[a] M(1) denotes the centroid of the ring C(1)−C(5).

Table 3. Selected Bond Angles (deg) for 1−3

1		2		3	
M(1)−Ge−M(1)′[a]	180.0	M(1)−Sn−M(1)′	180.0	M(1)−Pb−M(1)′	180.0
C(1)−Si−C(10)	112.6(3)	C(1)−Si−C(10)	112.0(2)	C(1)−Si−C(10)	111.7(2)
C(1)−Si−C(11)	112.3(3)	C(1)−Si−C(11)	112.3(2)	C(1)−Si−C(11)	111.7(3)
C(1)−Si−C(12)	109.6(2)	C(1)−Si−C(12)	110.7(2)	C(1)−Si−C(12)	110.6(2)
C(10)−Si−C(11)	104.8(3)	C(10)−Si−C(11)	104.3(3)	C(10)−Si−C(11)	104.8(3)
C(10)−Si−C(12)	108.6(3)	C(10)−Si−C(12)	108.9(3)	C(10)−Si−C(12)	109.4(3)
C(11)−Si−C(12)	108.6(3)	C(11)−Si−C(12)	108.3(3)	C(11)−Si−C(12)	108.6(3)
Si−C(1)−C(2)	126.3(4)	Si−C(1)−C(2)	126.9(3)	Si−C(1)−C(2)	127.0(4)
Si−C(1)−C(5)	127.2(3)	Si−C(1)−C(5)	127.4(3)	Si−C(1)−C(5)	127.1(4)
C(2)−C1)−C(5)	106.2(4)	C(2)−C(1)−C(5)	105.6(4)	C(2)−C(1)−C(5)	105.9(4)
C(1)−C(2)−C(3)	109.0(4)	C(1)−C(2)−C(3)	109.5(4)	C(1)−C(2)−C(3)	109.5(4)
C(1)−C(2)−C(6)	128.6(5)	C(1)−C(2)−C(6)	128.0(4)	C(1)−C(2)−C(6)	127.2(5)
C(3)−C(2)−C(6)	122.4(5)	C(3)−C(2)−C(6)	122.4(5)	C(3)−C(2)−C(6)	123.2(5)
C(2)−C(3)−C(4)	107.7(5)	C(2)−C(3)−C(4)	107.9(4)	C(2)−C(3)−C(4)	107.3(5)
C(2)−C(3)−C(7)	127.3(6)	C(2)−C(3)−C(7)	127.6(5)	C(2)−C(3)−C(7)	127.9(5)
C(4)−C(3)−C(7)	124.8(5)	C(4)−C(3)−C(7)	124.3(5)	C(4)−C(3)−C(7)	124.5(5)
C(3)−C(4)−C(5)	108.8(5)	C(3)−C(4)−C(5)	108.0(4)	C(3)−C(4)−C(5)	108.0(5)
C(3)−C(4)−C(8)	125.7(5)	C(3)−C(4)−C(8)	125.5(5)	C(3)−C(4)−C(8)	123.9(5)
C(5)−C(4)−C(8)	125.4(6)	C(5)−C(4)−C(8)	126.4(5)	C(5)−C(4)−C(8)	127.9(5)
C(1)−C(5)−C(4)	108.3(4)	C(1)−C(5)−C(4)	109.0(4)	C(1)−C(5)−C(4)	109.2(4)
C(1)−C(5)−C(9)	127.3(5)	C(1)−C(5)−C(9)	127.5(4)	C(1)−C(5)−C(9)	127.4(5)
C(4)−C(5)−C(9)	124.4(5)	C(4)−C(5)−C(9)	123.5(5)	C(4)−C(5)−C(9)	123.4(5)
Si−C(12)−C(13)	110.7(4)	Si−C(12)−C(13)	110.7(4)	Si−C(12)−C(13)	110.9(4)
Si−C(12)−C(14)	111.2(4)	Si−C(12)−C(14)	110.3(4)	Si−C(12)−C(14)	110.5(4)
Si−C(12)−C(15)	110.6(4)	Si−C(12)−C(15)	110.3(4)	Si−C(12)−C(15)	109.6(4)
C(13)−C(12)−C(14)	108.2(5)	C(13)−C(12)−C(14)	107.6(5)	C(13)−C(12)−C(14)	107.8(5)
C(13)−C(12)−C(15)	108.0(5)	C(13)−C(12)−C(15)	109.0(5)	C(13)−C(12)−C(15)	109.2(5)
C(14)−C(12)−C(15)	109.4(5)	C(14)−C(12)−C(15)	108.8(5)	C(14)−C(12)−C(15)	108.7(5)

[a] M(1) denotes the centroid of the ring C(1)−C(5).

Table 4. Selected Data for X-ray Crystallographically Characterized Ge^n Metallocenes

compd	M−Ge−M′ angle (deg)	M−Ge dist (Å)
[Ge(η^5-C_5H_5)$_2$][26]	152.4	2.234
[Ge(η^5-$C_5(CH_2Ph)_5$)$_2$][13,27]	162.6	2.239
[Ge(η^5-C_5H_9)-1,3-(SiMe$_3$)$_2$)-(η^5-C_5Me_5)][28]	163.0	2.439,[a] 2.066[b]
[Ge(η^5-C_5H_2-1,2,4-(SiMe$_3$)$_3$)$_2$][29]	169.5	2.256, 2.260
	171.8	2.251, 2.250
[Ge(η^5-Cp^s)$_2$]	180.0	2.210

[a] η^5-1,3-(SiMe$_3$)$_2$C$_5$H$_9$. [b] η^5-C$_5$Me$_5$.

Table 5. Selected Data for X-ray Crystallographically Characterized Sn^n Metallocenes

compd	M−Sn−M′ angle (deg)	M−Sn dist (Å)
[Sn(η^5-C_5H_5)$_2$][30]	146	2.401
[Sn(η^5-C_5Me_5)$_2$][31]	155	2.400, 2.399
[Sn(η^5-$C_5H_4P(NPr^i_2)_2$)$_2$][32]	150	2.379, 2.387
[Sn(η^5-C_5Ph_5)(η^5-C_5H_5)][33]	151	2.487,[a] 2.391[b]
[Sn(η^5-$C_5(CH_2Ph)_5$)$_2$][34]	156	2.439, 2.415
[Sn(η^5-C_5H_2-1,2,4-(SiMe$_3$)$_3$)$_2$][35]	162	2.280, 2.680
[Sn(η^5-C_5Me_4(SiMe$_3$))$_2$][9]	163.5	2.396
[Sn(η^5-$C_5H(C_3H_7)_4$)$_2$][36]	165	2.423, 2.424
[Sn(η^5-C_5Ph_5)$_2$][37]	180	2.401
[Sn(η^5-$C_5(CHMe_2)_5$)$_2$][7]	180	2.49
[Sn(η^5-Cp^2)$_2$]	180	2.379

[a] η^5-C$_5$Ph$_5$. [b] η^5-C$_5$H$_5$.

the cyclopentadienyl ligand. An energy level diagram of the frontier orbitals of $^-$Cp^s, $^-$C$_5$H$_5$, and $^-$C$_5$H$_4$(SiH$_3$) is shown in Figure 2. From an examination of the $^-$C$_5$H$_4$(SiH$_3$) ligand the effects of the silicon rather than the alkyl substituents may be distinguished. The main difference between the frontier orbitals of $^-$C$_5$H$_5$ and $^-$C$_5$H$_4$(SiH$_3$) is that the degeneracy of each e level is disrupted by the presence of the silyl substituent. This arises from the interaction between the $a_1(\pi)$, $e_2(\sigma)$, and $e_1(\sigma)$ levels of $^-$C$_5$H$_5$ and the sp^3 orbitals of the SiH$_3$ group. The second difference is the appearance in the manifold of the $^-$C$_5$H$_4$(SiH$_3$) ligand of two levels which are derived from the mixing of the a_1 level of $^-$C$_5$H$_5$ and one of the SiH$_3$ sp^3 orbitals and results in one of the new a_1-derived levels lying between the split $e_2(\sigma)$ level. The isosurfaces for these new a_1-derived levels and their schematic representation are shown in Figure 3. This

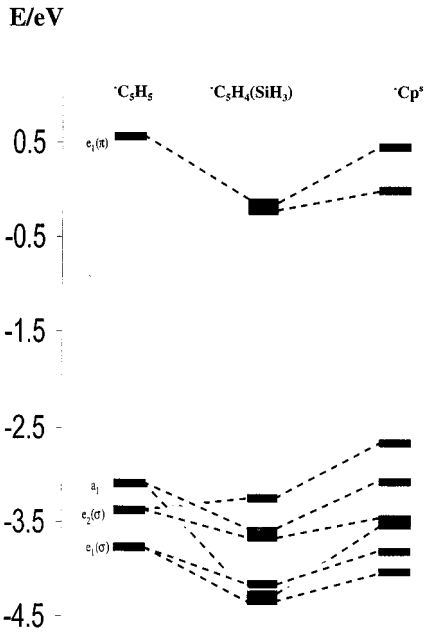

Figure 2. Energy level diagram of $^{-}C_5H_5$, $^{-}C_5H_4(SiH_3)$, and $^{-}Cp^s$.

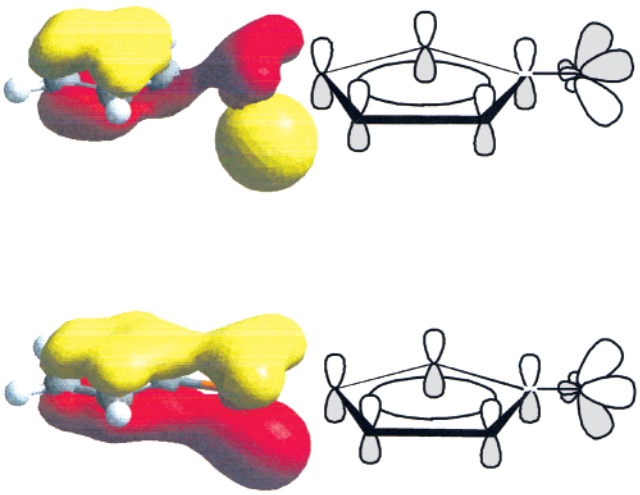

Figure 3. Isosurfaces and schematic representations of the $^{-}C_5H_4(SiH_3)$ a_1-derived levels.

Table 6. Selected Data for X-ray Crystallographically Characterized Pb^n Metallocenes

compd	M−Pb−M′ angle (deg)	M−Pb dist (Å)
$[Pb(\eta^5\text{-}C_5H_5)_2]$[38,39]	120	2.502, 2.820
$[Pb(\eta^5\text{-}C_5Me_5H)_2]$[40]	151	2.523, 2.479
$[Pb\{\eta^5\text{-}C_5(CH_2Ph)_5\}_2]$[41]	153	2.507, 2.500
$[Pb\{\eta^5\text{-}C_5Me_4(SiMe_3\}_2]$[9]	159	2.478, 2.500
$[Pb(\eta^5\text{-}Cp^s)_2]$[34]	180	2.460

reordering of the σ and π energy levels is retained in the frontier orbitals of the highly alkylated $^{-}Cp^s$ ligand, which differs from that of the $^{-}C_5H_4(SiH_3)$ manifold only by the degree of splitting of the e levels and by a general decrease in stability of all the levels. An examination of the isosurfaces of $^{-}Cp^s$, shown in Figure 4, reveals that the interactions involving the SiH_3 sp^3 orbitals are replaced by those of the Si−C sp^3 orbitals. The most dramatic consequence of these interactions between the cyclopentadienyl ring and the silyl substituents of $^{-}C_5H_4(SiH_3)$ and $^{-}Cp^s$ is reflected in the charges on C(1),

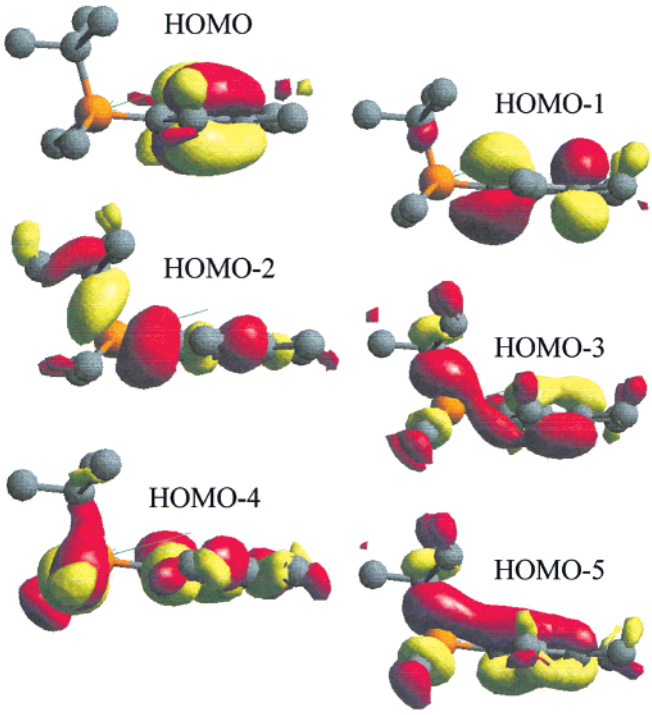

Figure 4. Isosurfaces of the $^{-}Cp^s$ ligand.

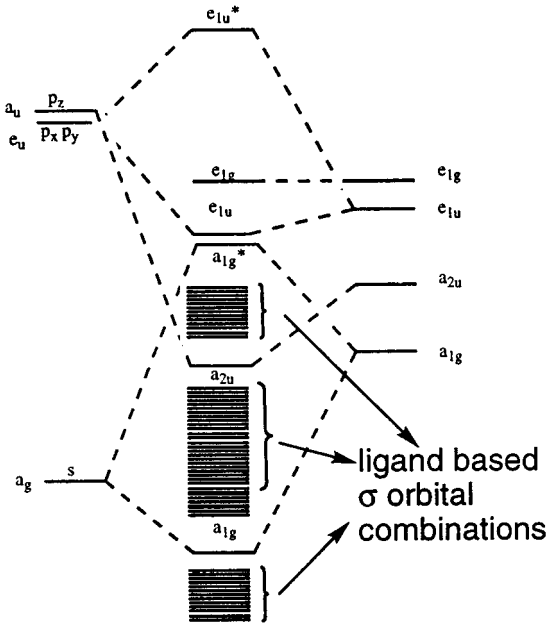

Figure 5. Molecular orbital diagrams of **1**−**3** labeled in D_{5d} symmetry.

the ring C bearing these groups, which are −0.36 and −0.35 respectively, compared to −0.11 for $^{-}C_5H_5$.

The MO diagram for **1**−**3** is shown in Figure 5. The manifold consists of 93 MOs. To facilitate comparisons with the results of others the MO diagram is labeled in D_{5d} symmetry, although C_i was established for **1** and **3** and C_{2h} symmetry for **2**. The two main metal−ligand bonding interactions are represented by the a_{1g} and a_{2u} levels (ca. −13 eV (orbital 29) and −9 eV (orbital 72), respectively). Their isosurfaces are shown in Figure 6 and represent the bonding combination of the ligand a_{1g} and a_{2u} orbitals and the s and p_z metal orbitals, respectively. The antibonding combination of the ligand a_{1g} and the metal s orbital is designated as a_{1g}*,

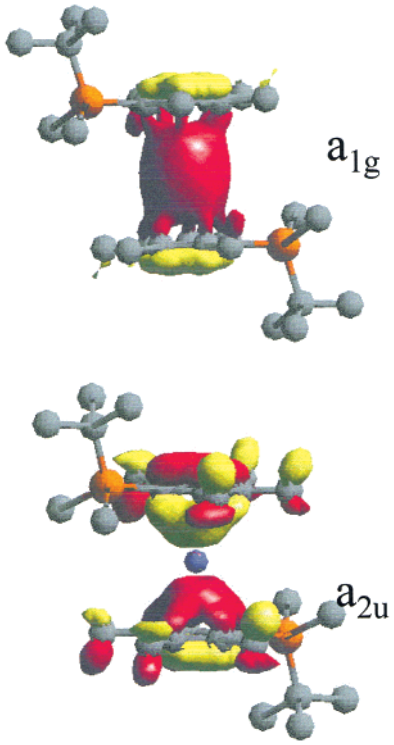

Figure 6. Isosurfaces of the a_{1g} and a_{2u} bonding orbitals of **2**.

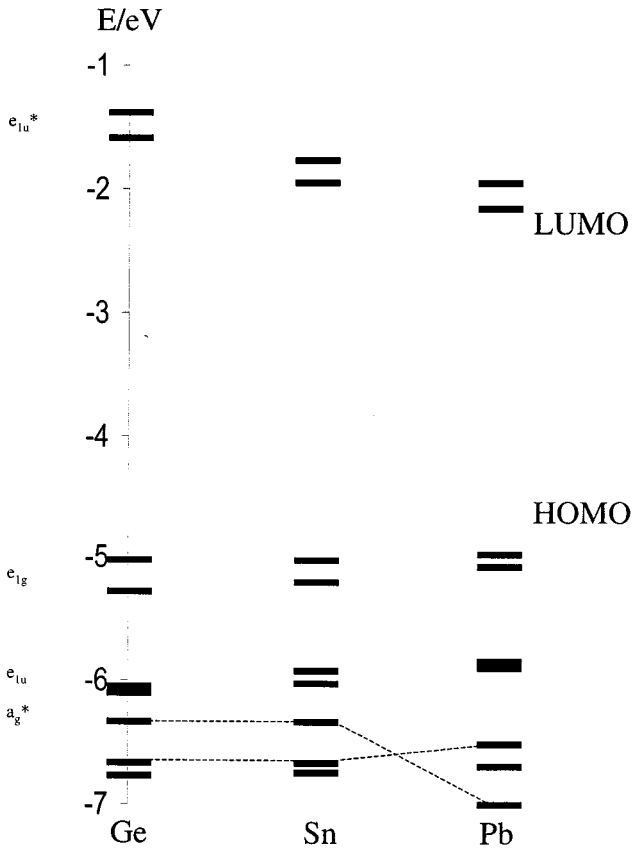

Figure 7. Energy level diagrams of **1**−**3**.

although this is sometimes labeled as $2a_{1g}$. Interleaved between the a_{1g}* and the a_{1g} and a_{2u} levels are two series of ligand-based σ orbitals. The first series contains approximately 20 orbitals, while the second contains approximately 40 (cf. 4 and 0, respectively, for their C_5H_5 analogues). The only other metal−ligand bonding interactions are observed in the frontier orbitals and are derived from a combination of the metal p_x and p_y orbitals with the e_{1u} combinations of the Cp^s ligand orbitals. The LUMO and SLUMO are composed of the antibonding combination of the metal p_x and p_y orbitals and the e_{1u} combination of the cyclopentadienyl p orbitals.

For group 14 metallocenes the a_{1g}* orbital has attracted the most interest, since it is essentially composed of the 4s, 5s, and 6s metal-based orbital of Ge, Sn, and Pb, respectively, and has antibonding ligand character. It has been proposed that the mixing of this metal-based lone pair and the metal p_x orbital, thereby producing a stereochemically active lone pair, is the driving force in causing Ge-based metallocenes to bend. This postulate was supported by the lack of any structurally characterized parallel metallocenes of Ge, although all calculations to date show the differences in energies between parallel and bent configurations for all three metallocenes are minimal (e.g. 6.4, 4, and 0.66 kcal mol^{-1} for Ge, Sn, and Pb, respectively[11]). Indeed for $[Ge(\eta^5\text{-}C_5H_5)_2]$,[12] it was shown that the energy of the a_{1g}* level varied inversely with the Ge−centroid distance and at values less than 2.337 Å lay above the e_{1u} level. Thus, for **1**, for which the Ge−centroid distance is 2.211 Å and for which the Cp^s rings are parallel, it was of interest to determine how the relative stability of this orbital compared to its analogues in both **2** and **3** and also that of $Ge(\eta^5\text{-}C_5H_5)_2$ with both bent (C_{2v}) and parallel (D_{5d}) geometries.

The energy levels of the frontier orbitals of **1**−**3** are shown in Figure 7, and in the case of **2**, the typical isosurfaces for these orbitals are shown in Figure 8. For all three metallocenes a_{1g}* lies below e_{1u}. It is also noteworthy that the stabilities of this orbital are approximately the same for Ge and Sn, whereas for Pb it is more stable by some 0.65 eV. The enhanced stability of the Pb-based lone pair derives from both a greater stabilization due to the relativistic correction and, as a consequence of this lower energy, a repulsion due to the like symmetry of this a_{1g}* orbital and an $a_g(\sigma)$ ligand-based orbital. Thus, for **3**, the a_{1g}* and this $a_g(\sigma)$ level cross over while the accompanying $a_u(\sigma)$ level remains unchanged. For the HOMO the degeneracy of the e level is disrupted by the presence of the silyl substituent, such that the combination which contain a nodal plane through C(1) is always higher in energy that that which does not. Finally, the LUMO and SLUMO increase in stability upon descending the group.

A Mulliken population analysis of **1**−**3** revealed that all three metal atoms possess a charge of ca. +1 (Table 7). The increase in charge upon descending the group is consistent with previous reports and arises due to the increased ionic nature of the bonding in **3** with respect to that in **1**, which results in a lower s population for **3** (Table 8). For all three parallel metallocenes the p population is essentially one electron. With the exception of Ge, for which the 4d level is more readily

(11) Armstrong, D. R.; Duer, M. J.; Davidson, M. G.; Moncrieff, D.; Russell, C. A.; Stourton, C.; Steiner, A.; Stalke, D.; Wright, D. S. *Organometallics* **1997**, *16*, 3340.
(12) Almöf, J.; Fernholt, L.; Fægri, K., Jr.; Haaland, A.; Schilling, B. E. R.; Seip, R.; Taugbøl, K. *Acta Chem. Scand.* **1983**, *A37*, 131.

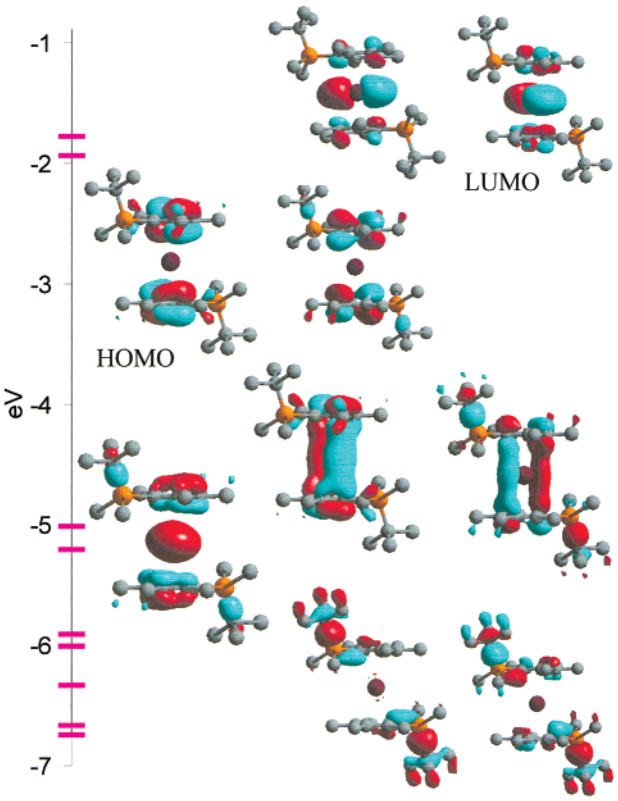

Figure 8. Isosurfaces for the LUMOs and the seven HOMOs of **2**.

Table 7. Mulliken Charges of Selected Atoms of 1−3

atom	1	2	3
metal	0.8340	0.9124	1.2618
Si	0.4644	0.5061	0.3951
C(1)	−0.3715	−0.4054	−0.3983
C(2)	−0.1800	−0.2103	−0.2076
C(3)	−0.1625	−0.1868	−0.1967
C(4)	−0.1518	−0.1868	−0.1960
C(5)	−0.1869	−0.2103	−0.2065
C(6)	0.0673	0.1170	0.0322
C(7)	0.0922	0.1120	0.0567
C(8)	0.0745	0.1120	0.0380
C(9)	0.0915	0.1170	0.0387
C(10)	−0.2285	−0.2222	−0.2704
C(11)	−0.2138	−0.2222	−0.2612
C(12)	−0.5992	−0.6001	−0.5799
C(13)	0.1576	0.1418	0.0935
C(14)	0.1483	0.1472	0.0865

Table 8. s, p, and d Populations of the Metal Atoms of 1−3

M	s	p	d
Ge	1.9588	1.0786	0.1287
Sn	1.9757	1.1008	0.0110
Pb	1.6547	1.0672	0.0162

accessible, little or no population of the d orbitals is observed.

As described above, the replacement of a C-centered substituent by the less electronegative Si-based $SiMe_2$-Bu^t results in the almost 2-fold increase in the formal negative charge on C(1) of ca. −0.4 e, relative to that of the other four CH_3-bearing C atoms (Table 7). The localization of this negative charge accounts for (a) the tendency of the more electropositive metal centers to "slip" toward this C(1) as observed in $[TiCp^s_2]$[13] and (b)

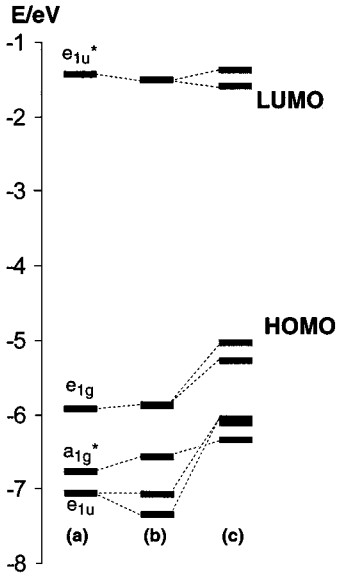

Figure 9. Comparison of the energy level diagrams of the frontier orbitals of (a) $Ge(C_5H_5)_2$ (D_{5d}), (b) $Ge(C_5H_5)_2$ (C_{2v}), and (c) **1** for Ge−cent = 2.211 Å.

the stability of the η^1 binding mode, again to C(1), displayed in both $[HgCp^s_2]$ and $[HgCp^sCl]$.[14]

A comparison of **1** and the parallel (D_{5d}) and bent (C_{2v}) forms of its C_5H_5 analogue was made. For the bent (C_{2v}) $Ge(C_5H_5)_2$ structure a geometry-optimized structure was obtained which agreed well with experimental data (Ge−cent = 2.236 Å (2.234 Å) and cent−Ge−cent = 151.82° (152.36°)). Single-point energy calculations were also performed on a second C_{2v} structure having a Ge−cent distance identical with that observed for **1** (2.211 Å). Three D_{5d} structures were examined with Ge−cent distances of 2.211, 2.234, and 2.337 Å. In accord with the results of previous workers,[12] we find that (i) for $Ge(C_5H_5)_2$, the D_{5d} structure is most stable when Ge−cent = 2.337 Å and this structure is more stable than the geometry-optimized C_{2v} structure by 0.067 eV and that (ii) the stability of the a_{1g}* level decreased with decreasing metal−cent distance and at 2.211 Å lay above the e_{1u} level in both the C_{2v} and D_{5d} isomers. A comparison of energy level diagrams of the frontier orbitals of **1** with those of $Ge(C_5H_5)_2$ (both D_{5d} and C_{2v} forms with Ge−cent = 2.211 Å) is shown in Figure 9. For **1** the a_{1g}* level is similar in energy to that of its unsubstituted counterparts, whereas the e levels are higher. Thus, the reordering of the manifold for **1** compared with $Ge(C_5H_5)_2$ results from the decreased stability of the e_{1g} and e_{1u} orbitals which arises from the increased charge on the Cp^s ligand. A comparison of the Mulliken populations of $Ge(C_5H_5)_2$ and **1** is presented in Table 9. This reveals that there is a greater charge on the parallel structures and that in addition the Cp^s ligands generate a further 20% increase in charge at the Ge center.

NMR Spectroscopy of $[M(\eta^5\text{-}Cp^s)_2]$. The ^1H NMR spectrum of **2** in C_6D_6 exhibits four resonances in the ratio 6:6:9:6, at δ 2.07, 1.95, 0.97, and 0.32, respectively. The $^{13}C\{^1H\}$ NMR spectrum displays eight chemically

(13) Hitchcock, P. B.; Kerton, F. M.; Lawless, G. A. *J. Am. Chem. Soc.* **1998**, *120*, 10264.
(14) Hitchcock, P. B.; Keates, J. M.; Lawless, G. A. *J. Am. Chem. Soc.* **1998**, *120*, 599.

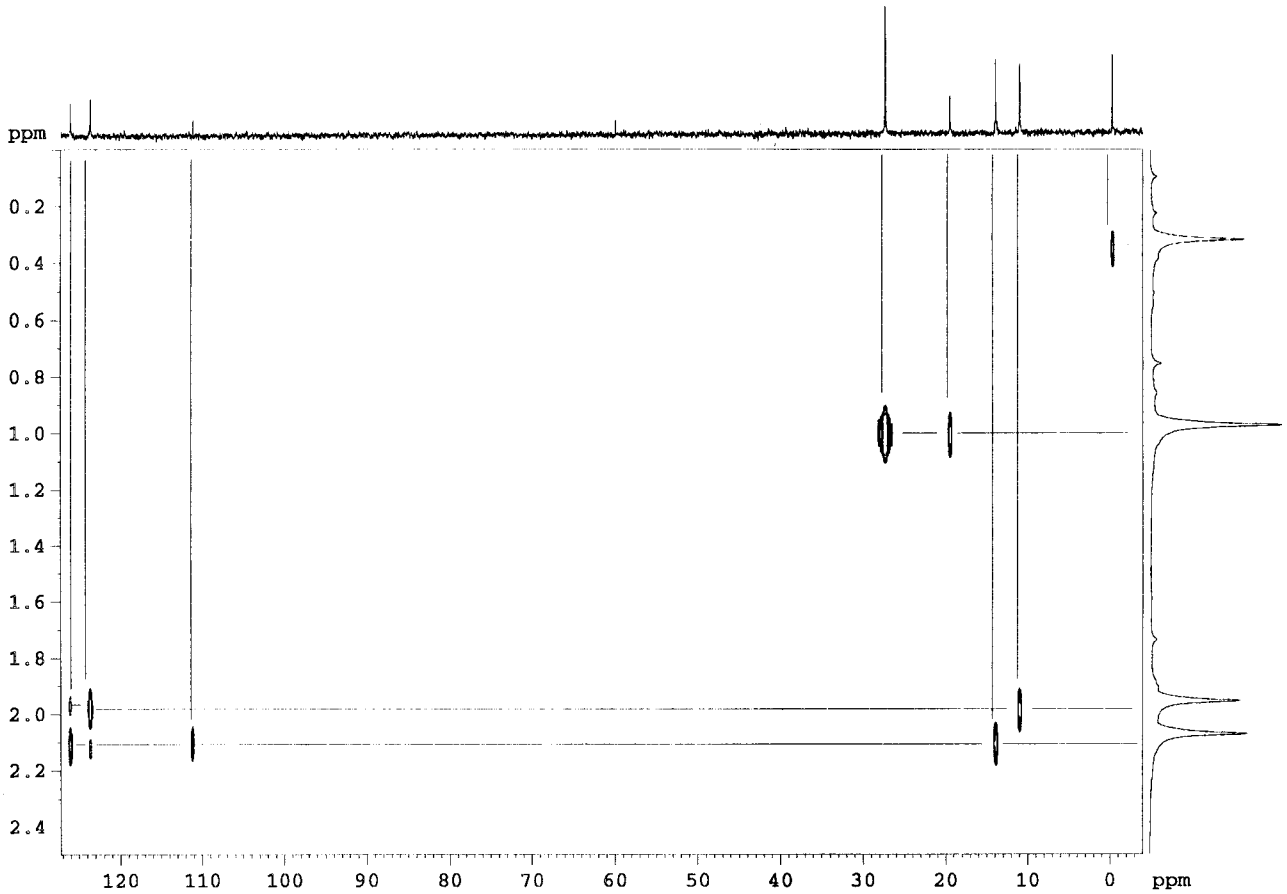

Figure 10. $^{1}H-^{13}C$ COLOC NMR spectrum of **2**.

Table 9. Mulliken Charges and Populations of 1 and $Ge(C_5H_5)_2$ at Various Ge−cent Distances

			population		
compd (sym)	Ge−cent (Å)	charge	s	p	d
$GeCp_2$ (D_{5d})	2.211	0.705	1.943	1.207	0.145
	2.234	0.711	1.941	1.207	0.141
	2.337	0.735	1.935	1.206	0.124
$GeCp_2$ (C_{2v})	2.211	0.694	1.932	1.229	0.144
	2.236	0.688	1.914	1.264	0.133
1	2.211	0.834	1.959	1.079	0.129

Table 10. Assignment of ^{1}H and ^{13}C Resonances for 2

$\delta(^{1}H)$	assignt	$\delta(^{13}C)$	assignt
0.32	$Si-CH_3$	0.28	C(10,11)
0.97	$C-(CH_3)_3$	11.02	C(7,8)
1.95	$C(3,4)-CH_3$	13.92	C(6,9)
2.07	$C(2,5)-CH_3$	19.48	C(12)
		27.35	C(13−15)
		111.19	C(1)
		123.64	C(3,4)
		126.07	C(2,5)

distinct ^{13}C environments and displays couplings to both ^{29}Si and $^{119(117)}Sn$. The ^{13}C resonances of the Cp^s rings were observed at δ 126.08, 123.64, and 111.18 (C(2,5), C(3,4) and C(10), respectively) with $^{1}J(^{119(117)}Sn-^{13}C)$ couplings of 20, 10, and ca. 56 Hz, respectively. For the last resonance the resolution of the $^{1}J(^{119}Sn-^{13}C)$ and $^{1}J(^{117}Sn-^{13}C)$ couplings was possible. The two ^{13}C resonances of the Bu^t groups were observed at δ 27.35 and 19.48 (C(13−15) and C(12) respectively), with a $^{1}J(^{29}Si-^{13}C)$ coupling of 56 Hz observed for the latter. Three resonances were observed for the Me groups at δ 13.92 and 11.02 (C(6−9)) and at δ −0.28 (C(10,11)) with $^{2}J(^{119(117)}Sn-^{13}C)$ couplings of 22 Hz and a $^{1}J(^{29}Si-^{13}C)$ coupling of 50.6 Hz observed, respectively. The $^{13}C\{^{1}H\}$ CP MAS solid-state NMR spectrum of **2** compares favorably with those of the solution-state spectrum: δ 124, individual resonances due to C(2,5) and C(3,4) were not resolved, δ 109, C(1); δ 27, C(13−15); δ 20, C(12); δ 13 and 11, C(6−9); δ 0, C(10,11). More importantly, the observation of only seven chemically distinct ring C environments of the Cp^s ligand in the solid state confirms the presence of a reflection plane or an inversion center in the molecule.

A COLOC (COrrelation spectroscopy via LOng-range Coupling) 2-D heteronuclear correlation technique was performed in order to assign unambiguously the ^{1}H and ^{13}C resonances of the $^{-}C_5Me_4(SiMe_2Bu^t)$ ligand (Figure 10). The ^{1}H resonance at δ 0.32 showed a single, strong correlation to the ^{13}C resonance at δ −0.28, while the ^{1}H resonance at δ 0.97 displayed a strong correlation with the ^{13}C resonance at δ 27.35 ($^{1}J(^{1}H-^{13}C)$) and a weaker correlation with the ^{13}C resonance at δ 19.48 ($J(^{1}H-^{13}C)$). The ^{1}H resonance at δ 2.07 exhibited a strong correlation with the ^{13}C signal at δ 13.92 and three weaker correlations to the resonances at δ 126.07 ($^{2}J(^{1}H-^{13}C)$) and δ 123.64 and 111.19 (both $^{3}J(^{1}H-^{13}C)$). Finally, for the ^{1}H resonance at δ 1.95 a strong correlation with the ^{13}C resonance at δ 11.02 ($^{1}J(^{1}H-^{13}C)$) and two weaker correlations to the signals at δ 123.64 ($^{2}J(^{1}H-^{13}C)$) and δ 126.07 ($^{3}J(^{1}H-^{13}C)$) were observed. On the basis of these observations the ^{1}H and ^{13}C spectra were assigned (listed in Table 10), and since

Table 11. Selected ^{119}Sn and ^{207}Pb NMR Solution and Solid-State Chemical Shift Data for Sn^{II} and Pb^{II} Metallocenes

compd	$\delta(^{119}Sn)$	$\delta_{iso}(^{119}Sn)$	compd	$\delta(^{119}Pb)$	$\delta_{iso}(^{119}Pb)$
$[Sn(\eta^5\text{-}C_5Me_5)_2]$	−2129[42]	−2140[43]	$[Pb(\eta^5\text{-}C_5Me_5)_2]$	−4390[15]	−4474[43]
$[Sn(\eta^5\text{-}C_5(CH_2Ph)_5)_2]$[17]	−2188	−2288	$Pb[\eta^5\text{-}C_5Me_4(SiMe_2(C_5HMe_4))]_2$[44]	−4538	
$[Sn(\eta^5\text{-}C_5H_5)_2]$	−2199[45]	−2163, −2224[45]	**3**	−4595	−4692
$[Sn(\eta^5\text{-}C_5Ph_5)_2]$[47]		−2215	$Pb(\eta^5\text{-}C_5H_3Bu^t_2)_2$[48]	−4756	
$[Sn(\eta^5\text{-}C_5Me_4(SiMe_3))_2]$[10]	−2171	−2203	$[Pb(\eta^5\text{-}C_5H_5)_2]$[43]	−5030	
2	−2204		$[Pb(\eta^5\text{-}C_5Ph_5)_2]$[47]		−6150

Table 12. Comparison of Solution-State Coupling Constants, ^nJ(M−C) (in Hz), for 2 and 3

^nJ(M−C)	**2**	**3**
C(3) ^1J(M−C)	10	40
C(2) ^1J(M−C)	20	41
C(1) ^1J(M−C)	^{119}Sn, 56; ^{117}Sn, 53.5	82
C(1) $^1J(^{29}Si-C)$	70	not obsd
$C(CH_3)_3$ $^1J(^{29}Si-C)$	56	not obsd
C(2)(CH_3) ^{2}(M−C)	21	22
C(3)CH_3) ^2J(M−C)	21	23
Si(CH_3) ^1J(Si−C)	50	50

compounds **1** and **3** displayed essentially identical ^{1}H and ^{13}C{^{1}H} spectra, these assignments were extended to their spectra also. The solution- and solid-state ^{29}Si-{^{1}H} NMR spectra of **1**−**3** all exhibited a single resonance, at ca. δ −2. The values for the ^{119}Sn{^{1}H} chemical shifts of **2** in solution and in the solid state (δ −2204 and δ_{iso} −2236, respectively) compare favorably, both with chemical shifts recorded for other metallocenes of Sn^{II} and with each other (Table 11). The latter suggests that there is little or no structural deviation between the solution and solid states, i.e. no reduction in hapticity of the cyclopentadienyl rings. The ^1J(M−C) and ^2J(M−C) values for **2** and **3** (Table 12) are in close agreement with previous studies.[15] The increased magnitude of ^1J(M−C(1)) is in good agreement with the calculated greater s electron density at this carbon center and the observed short M−C(1) distance. The ^{207}Pb{^{1}H} chemical shift values observed for **3** (Figure 11) in solution and in the solid state (δ −4595 and δ_{iso} −4692, respectively) are similar to one another and close to the values reported for $[Pb(\eta\text{-}C_5Me_5)_2]$.[16] Although no solution-state ^{207}Pb NMR data have been reported for $Pb(\eta\text{-}C_5Ph_5)_2$, presumably due to its insolubility in common organic solvents, the solid-state ^{207}Pb δ_{iso} value has been reported as −6150.[17] The large difference between this value and that of **3** cannot be due to a substantial difference in their respective molecular structures. For example, the corresponding ^{119}Sn{^{1}H} δ_{iso} values for **2** and $[Sn(\eta\text{-}C_5Ph_5)_2]$ differ by just 21 ppm and moreover, on the basis of these data, the predicted ^{207}Pb chemical shifts for **3** and $Pb(\eta\text{-}C_5Ph_5)_2$ should be δ_{iso} −5043 and −4974, respectively. Thus, we propose that the original assignment of δ_{iso} for $Pb(\eta\text{-}C_5Ph_5)_2$ is in error and is most probably due to the large chemical shift anisotropy (csa) associated with solid-state ^{207}Pb NMR spectroscopy. This large csa is evident from the large number of spinning sidebands observed even at spin rates of 15 kHz (Figure 11).

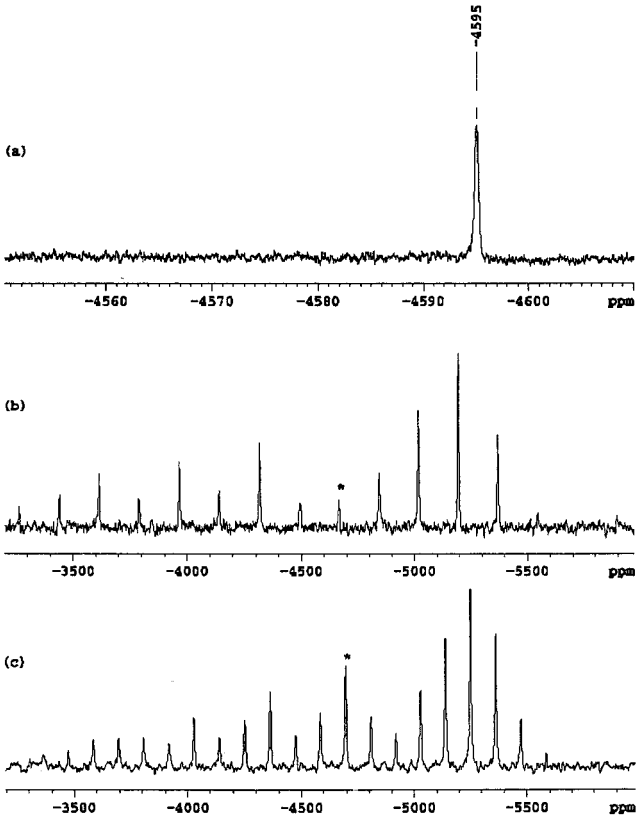

Figure 11. ^{207}Pb{^{1}H} NMR spectra of **3** (δ_{iso} indicated by asterisks): (a) solution and CP MAS solid state; (b) ν_r = 15 kHz; (c) ν_r = 9.5 kHz.

Conclusions

We have synthesized and structurally characterized the first series of isomorphous group 14 metallocenes. It is noteworthy that (i) **1** and **3** are the first examples of structurally characterized parallel metallocenes of Ge and Pb while **2** was only the second such example for Sn, (ii) **1** is the first example of a Ge-based molecule to contain a stereochemically inactive lone pair of electrons, and (iii) the a_{1g}* orbitals of **1**−**3** are lower in energy than their respective e_{1u} orbitals, which is the reverse of what is observed in their C_5H_5 analogues.

Experimental Section

General Considerations. Air-sensitive compounds were handled with rigorous exclusion of oxygen and water under an atmosphere of dry dinitrogen using Schlenk-type glassware on a dual-manifold Schlenk line or under a dry dinitrogen atmosphere in a Braun AG glovebox operating at <1 ppm of H_2O and <1 ppm of O_2. Elemental analyses (C, H) were performed by MEDAC. Solvents were purified by distillation from appropriate drying agents under an atmosphere of dry dinitrogen.[18] LiBu^n (2.5 mol dm^{-3} in hexane) and LiBu^t (1.7 mol dm^{-3} in pentane) were purchased from Aldrich Chemical

(15) Jutzi, P.; Dickbreder, R.; Nöth, H. *Chem. Ber.* **1989**, *122*, 865.
(16) Wrackmeyer, B.; Sebald, A.; Merwin, L. H. *Magn. Reson. Chem.* **1991**, *29*, 260.
(17) Janiak, C.; Schumann, H.; Stader, C.; Wrackmeyer, B.; Zuckerman, J. J. *Chem. Ber.* **1988**, *121*, 1745.

Co. The compound $C_5H_2Me_4$ was prepared according to literature procedures.[19,20] ^{1}H, ^{13}C, ^{29}Si, ^{119}Sn, and ^{207}Pb NMR spectra were run on a Bruker DMX-400 instrument (89 mm wide-bore magnet) at a field of 9.395 T. Chemical shifts are reported in parts per million (δ) with $SiMe_4$ (^{1}H, ^{13}C, and ^{29}Si spectra), $SnMe_4$ (^{119}Sn spectra), and $PbMe_4$ (^{207}Pb spectra) as external references.

Si(η^1-C_5HMe_4)Me_2Cl. LiC_5HMe_4 (13.84 g, 108.10 mmol) in thf (250 mL) was added to a three-necked 500 mL round-bottomed flask equipped with a stirbar and cooled to 0 °C. With stirring, over a 30 min period, $SiMe_2Cl_2$ (13.10 mL, 108.10 mmol) was added dropwise and the thick white slurry thinned to a clear, pale yellow solution. After it was stirred for a further 2 h, the thf was removed in vacuo. Extraction with hexane (2 × 60 mL) afforded Si(η^1-C_5HMe_4)Me_2Cl as a sweet-smelling, O_2- and H_2O-sensitive pale yellow liquid ($\rho = 0.95$). Yield: 97% (22.44 g, 104.90 mmol). ^{1}H NMR (C_6D_6, 400.13 MHz): δ 3.09 (s, 1H), 1.99 (s, 6H), 1.83 (6H), 0.25 (s, 6H). ^{13}C{^{1}H} NMR (C_6D_6, 100.61 MHz): δ 138.22 (C(2)), 131.81 (C(3)), 56.78 (C(1)), 14.66 (C(2)−*C*H$_3$), 11.63 (C(3)−*C*H$_3$), 0.96 (Si−*C*H$_3$). ^{29}Si{^{1}H} NMR (C_6D_6, 79.49 MHz): δ 26.53.

LiCp^s. A Schlenk tube containing Si(η^1-C_5HMe_4)Me_2Cl (1.76 g, 8.20 mmol), thf (100 mL), and a stirbar was cooled to −78 °C using a dry ice/acetone slush bath. To this solution was added 2 equiv of LiBu^t (16.40 mmol, 1.70 mol dm^{-3} in pentane) with stirring over a 10 min period. Stirring was continued for 1 h, after which time the mixture was warmed to ambient temperature. Following stirring of the mixture for a further 2 h, the thf was removed in vacuo, the residue washed with cold hexane (3 × 50 mL), and the product extracted with Et_2O (3 × 60 mL) and washed once again with hexane (2 × 50 mL). Drying in vacuo afforded $LiCp^s_2$ as an O_2- and H_2O-sensitive fine white powder. Yield: 90% (1.79 g, 7.40 mmol). ^{13}C{^{1}H} NMR (C_6D_6/thf (5:95), 100.61 MHz): δ 117.28 (C(2)), 111.96 (C(3)), 97.50 (C(1)), 27.22 (C−(*C*H$_3$)$_3$), 14.52, 10.96, 0.85 (the resonance corresponding to *C*−(CH$_3$)$_3$ was obscured by solvent). ^{29}Si{^{1}H} NMR (C_6D_6/thf (5:95), 79.48 MHz): δ −4.90.

[GeCp$^s_2$] (1). A solution of $LiCp^s_2$ (0.64 g, 2.66 mmol) in thf (50 mL) was added, over a 2 min period with stirring, to a slurry of $GeCl_2$·diox (0.31 g, 1.33 mmol) and thf (50 mL). A slow color change from colorless to pale yellow was observed and was accompanied by the formation of a small amount of white precipitate. After 24 h of stirring, the thf was removed in vacuo and the product extracted with hexane (60 mL). Removal of the hexane in vacuo afforded **1** as small, pale yellow needles, which did not show any visible signs of decomposition in air. Yield: 97% (0.70 g, 1.29 mmol). Recrystallization from hot toluene afforded large pale yellow needles. Mp: 213.9 °C. ^{1}H NMR (C_6D_6, 400.13 MHz): δ 2.02 (s, 6H), 1.87 (s, 6H), 0.97 (s, 9H), 0.31 (s, 6H). ^{13}C{^{1}H} NMR (C_6D_6, 100.61 MHz): δ 127.18 (C(2)), 124.53 (C(3)), 113.01 (C(1)), 27.23 (C−(*C*H$_3$)$_3$]), 19.31 (*C*−(CH$_3$)$_3$), 13.61 (C(2)−*C*H$_3$), 10.85 (C(3)−*C*H$_3$), -0.64 (Si−*C*H$_3$). ^{29}Si{^{1}H} NMR (C_6D_6, 79.49 MHz): δ −1.62. EI MS: M$^{\bullet+}$ *m*/*z* 309 (100%), M$^{\bullet+}$ − Bu^t *m*/*z* 252 (7%), M$^{\bullet+}$ − Bu^t − Ge *m*/*z* 177 (18%). Anal. Calcd (found) for $C_{30}H_{54}Si_2Ge$: C, 65.88 (66.30); H, 9.71 (10.01).

[SnCp$^s_2$] (2). $LiCp^s_2$ (1.11 g, 4.60 mmol) dissolved in Et_2O (60 mL) was added, over a 2 min period with stirring, to a Schlenk tube charged with a slurry of $SnCl_2$ (0.38 g, 2.00 mmol) and Et_2O (30 mL). An immediate color change from white to yellow was accompanied by the formation of a white precipitate. After 12 h of stirring the Et_2O was removed in vacuo and the product extracted with hexane (50 mL). Removal of the hexane in vacuo afforded **2** as a yellow powder, only sensitive to O_2 and H_2O upon prolonged exposure. Yield: 89% (1.04 g, 1.77 mmol). Recrystallization from hexane afforded yellow needles. Mp: 177.8 °C. ^{1}H NMR (C_6D_6, 400.13 MHz): δ 2.07 (s, 6H), 1.95 (s, 6H), 0.97 (s, 9H), 0.32 (s, 6H). ^{13}C{^{1}H} NMR (C_6D_6, 100.61 MHz): δ 126.08 (C(2), ^1J(Sn−C) = 20 Hz), 123.64 (C(3), ^1J(Sn−C) = 10 Hz], 111.18 (C(1), ^1J(^{117}Sn−C) = 53.5 Hz, ^1J(^{119}Sn−C) = 56.3 Hz, ^1J(^{29}Si−C) = 70 Hz), 27.35 (C−(*C*H$_3$)$_3$), 19.48 (*C*−(CH$_3$)$_3$, ^1J(^{29}Si−C) = 56.5 Hz), 13.92 (C(2)−*C*H$_3$, ^2J(Sn−C) = 21.6 Hz), 11.02 (C(3)−*C*H$_3$, ^2J(Sn−C) = 21.8 Hz), −0.28 (Si−*C*H$_3$, ^1J(Si−C) = 50.6 Hz). ^{29}Si{^{1}H} NMR (C_6D_6, 79.49 MHz): δ −2.13. ^{119}Sn{^{1}H} NMR (C_6D_6, 148.91 MHz): δ −2204. ^{13}C{^{1}H} CP MAS NMR (400.13 MHz): δ 124 (C(2) and C(3) do not resolve), 109 (C(1)), 27 (C−(*C*H$_3$)$_3$), 20 (*C*−(CH$_3$)$_3$), 14 (C(2)−*C*H$_3$), 11 (C(3)−*C*H$_3$), 0 (Si−*C*H$_3$). ^{29}Si{^{1}H} CP MAS NMR (79.48 MHz): δ −3. ^{119}Sn{^{1}H} CP MAS NMR (148.91 MHz): δ −2236. EI MS: M$^{\bullet+}$ *m*/*z* 355 (100%), M$^{\bullet+}$ − Bu^t *m*/*z* 298 (9%), M$^{\bullet+}$ − Sn *m*/*z* 235 (27%), $C_5Me_4(SiMe_2Bu^t)^{\bullet+}$ − Bu^t *m*/*z* 178 (85%). Anal. Calcd (found) for $C_{30}H_{54}Si_2Sn$: C, 62.02 (61.11); H, 9.40 (9.23).

[PbCp$^s_2$] (3). A slurry of $PbCl_2$ (0.60 g, 2.15 mmol) in Et_2O (40 mL) was cooled to −78 °C using a dry ice/acetone slush bath, and to it was added $LiCp^s_2$ (1.04 g, 4.30 mmol) dissolved in Et_2O (40 mL), over a 2 min period with stirring. When the temperature was raised to ca. −20 °C, a color change from white to yellow was observed. After the mixture was stirred at ambient temperature for 2 h, a white precipitate was formed and the color of the solution changed to deep orange. After a further 2 h of stirring, **3** was obtained as a deep orange-red, crystalline material by filtration of the solution and removal of the Et_2O in vacuo. Yield: 84% (1.20 g, 1.80 mmol). Recrystallization from hexane/toluene afforded red needles, only sensitive to O_2 and H_2O upon very long exposure. Mp: 178.5 °C. ^{1}H NMR (C_6D_6, 400.13 MHz): δ 2.27 (s, 6H), 2.11 (s, 6H), 0.97 (s, 9H), 0.32 (s, 6H). ^{13}C{^{1}H} NMR (C_6D_6, 100.61 MHz): δ 127.05 (C(2), ^1J(Pb−C) = 41.3 Hz), 124.38 (C(3), ^1J(Pb−C) = 40.2 Hz), 111.09 (C(1), ^1J(Pb−C) = 82.3 Hz), 27.30 (C−(*C*H$_3$)$_3$), 19.86 (*C*−(CH$_3$)$_3$), 13.56 (C(2)−*C*H$_3$, ^2J(Pb−C) = 22.2 Hz), 10.66 (C(3)−*C*H$_3$, ^2J(Pb−C) = 23.5 Hz), −0.21 (Si−*C*H$_3$, ^1J(Si−C) = 50.4 Hz). ^{29}Si{^{1}H} NMR (C_6D_6, 99.33 MHz): δ −3.11. ^{207}Pb{^{1}H} NMR (C_6D_6, 83.69 MHz): δ −4595. ^{13}C CP-MAS (400.13 MHz): δ 130, 129 (C(2)), 128 (C(3), ^1J(Pb−C) = 60 Hz), 112 (C(1), ^1J(Pb−C) = 80 Hz), 30 (C−(*C*H$_3$)$_3$), 24 (*C*−(CH$_3$)$_3$), 16 (C(2)−*C*H$_3$), 14 (C(3)−*C*H$_3$), 4 (Si−*C*H$_3$). ^{29}Si CP-MAS (79.48 MHz): δ −1. ^{207}Pb CP-MAS (83.69 MHz): δ −4692. EI MS: M$^{\bullet+}$ *m*/*z* 678 (19%), M$^{\bullet+}$ − $C_5Me_4(SiMe_2Bu^t)$ *m*/*z* 443 (98%), M$^{\bullet+}$ − $C_5Me_4(SiMe_2Bu^t)$ − Pb *m*/*z* 235 (56%), M$^{\bullet+}$ − $C_5Me_4(SiMe_2Bu^t)$ − Pb − Bu^t *m*/*z* 178 (100%). Anal. Calcd (found) for $C_{30}H_{54}Si_2Pb$: C, 52.66 (53.14); H, 8.04 (8.03).

Crystallography. All structures were solved by direct methods and refined on F^2 by the full-matrix least-squares procedure.

Crystal Structure Data for 1. For $C_{30}H_{54}Si_2Ge$: T = 293(2) K, specimen 0.3 × 0.3 × 0.2 mm, M_r = 543.5, monoclinic, space group $P2_1/n$ (nonstandard No. 14), a = 13.207(4) Å, b = 8.781(4) Å, c = 13.844(3) Å, β = 92.25(2)°, V = 1604.3(9) Å^3, D_{calcd} = 1.13 g cm^{-3}, Z = 2, for reflections with $2 \le \theta \le 30°$, $R(F)$ = 0.084 for 1949 observed reflections ($I > 2\sigma(I)$) and $R_w(F^2)$ = 0.207 for all 4662 (R(int) = 0.0590) reflections.

Crystal Structure Data for 2. For $C_{30}H_{54}Si_2Sn$: T = 293(2) K, specimen 0.3 × 0.3 × 0.2 mm, M_r = 589.6, monoclinic, space group $P2_1/n$ (nonstandard No. 14), a = 13.126(2) Å, b = 9.135(7) Å, c = 13.769(2) Å, β = 92.41(10)°, V = 1649.5(13) Å^3, D_{calcd} = 1.19 g cm^{-3}, Z = 2, for reflections with $2 \le \theta \le 25°$, $R(F)$ = 0.043 for 1956 observed reflections ($I > 2\sigma(I)$) and $R_w(F^2)$ = 0.107 for all 2892 (R(int) = 0.0182) reflections.

Crystal Structure Data for 3. For $C_{30}H_{54}Si_2Pb$: T = 173(2) K, specimen 0.3 × 0.3 × 0.2 mm, M_r = 678.1, monoclinic, space group $P2_1/n$ (nonstandard No. 14), a = 12.945(3) Å, b = 9.219(4) Å, c = 13.661(4) Å, β = 93.96(2)°, V = 1626.4(9) Å^3, D_{calcd} = 1.39 g cm^{-3}, Z = 2, for reflections with $2 \le \theta \le 28°$, $R(F)$ = 0.044 for 2734 observed reflections ($I > 2\sigma(I)$) and $R_w(F^2)$ = 0.104 for all 3903 (R(int) = 0.0271) reflections.

Computational Details. The reported calculations were

(18) Perrin, D. D.; Armarego, W. L. F.; Perrin, D. R. *Purification of Laboratory Chemicals*, 2nd ed.; Pergamon: New York, 1988.
(19) Kohl, F. X.; Jutzi, P. *J. Organomet. Chem.* **1983**, *243*, 119.
(20) Fendrick, C. M.; Schertz, L. D.; Day, V. W.; Marks, T. J. *Organometallics* **1988**, *7*, 1828.

performed using the Amsterdam density functional (ADF) package.[21] The numerical integration procedure applied for the calculations is that of te Velde and Baerends.[22] A triple-ξ Slater type orbital (STO) basis set with a polarization function was used for describing the valence electrons of Ge (4s, 4p), Sn (5s, 5p), Pb (6s, 6p), and Si (3s, 3p). A double-ξ STO basis set augmented by a polarization function was used for C (2s, 2p) and H. Electrons in lower shells were treated with the frozen-core approximation. Energies of the structures **1**−**3** were calculated using the local density approximation (LDA) (due to Vosko et al.[23]). The nonlocal exchange of Becke,[24] the nonlocal correlation correction of Perdew,[25] and the scalar relativistic correction[26] were applied to the LDA density. All calculations were performed on an SG Indigo^2 Impact 10000.

Acknowledgment. H.C. thanks the Royal Society for the award of a Dorothy Hodgkin Research fellowship. We also wish to thank the EPSRC for financial support and Dow Corning for a CASE award (S.P.C.), Dr. M. P. Waugh and Dr. J. M. Keates for experimental aid, and Prof. J. N. Murrell for useful discussions.

Supporting Information Available: Tables of crystallographic data, atom coordinates, bond lengths and angles, and anisotropic thermal parameters for **1**. This material is available free of charge via the Internet at http://pubs.acs.org.

OM990884Z

(21) Baerends, E. J.; Ellis, D. E.; Ros, P. *Chem. Phys.* **1973**, *2*, 41.
(22) te Velde, G.; Baerends, E. J. *J. Comput. Phys.* **1992**, *99*, 84.
(23) Vosko, S. H.; Wilk, L.; Nusair, M. *Can. J. Phys.* **1980**, *58*, 1200.
(24) Becke, A. D. *Phys. Rev. A* **1988**, *38*, 2398.
(25) Perdew, J. P. *Phys. Rev. B* **1986**, *33*, 8822.
(26) Ziegler, T.; Tschinke, V.; Baerends, E. J.; Snijders, J. G.; Ravenek, W. *J. Phys. Chem.* **1989**, *93*, 3050.
(27) Grenz, M.; Hahn, E.; du Mont, W.-W.; Pickardt, J. *Angew. Chem., Int. Ed. Engl.* **1984**, *23*, 61.
(28) Schumann, H.; Janiak, C.; Hahn, E.; Loebel, J.; Zuckerman, J. J. *Angew. Chem., Int. Ed. Engl.* **1985**, *24*, 773.
(29) Cowley, A. H.; Mardones, M. A.; Avendano, S.; Roman, E.; Manriquez, J. M.; Carrano, C. J. *Polyhedron* **1993**, *12*, 125.
(30) Jutzi, P.; Schluter, E.; Hursthouse, M. B.; Arif, A. M.; Short, R. L. *J. Organomet. Chem.* **1986**, *299*, 285.
(31) Fischer, E. O.; Grubert, H. *Z. Naturforsch.* **1956**, *423*, B11.
(32) Jutzi, P.; Kohl, F. X.; Hoffmann, P.; Kruger, C.; Tsay, Y. *Chem. Ber.* **1980**, *113*, 757.
(33) Cowley, A. H.; Lasch, J. G.; Norman, N. C.; Stewart, C. A.; Wright, T. C. *Organometallics* **1983**, *2*, 1691.
(34) Heeg, M. J.; Herber, R. H.; Janiak, C.; Zuckerman, J. J.; Schumann, H.; Manders, W. F. *J. Organomet. Chem.* **1988**, *346*, 321.
(35) Schumann, H.; Janiak, C.; Hahn, E.; Kolax, C.; Loebel, J.; Rausch, M. D.; Zuckerman, J. J.; Heeg, M. J. *Chem. Ber.* **1986**, *119*, 2656.
(36) Cowley, A. H.; Jutzi, P.; Kohl, F. X.; Lasch, J. G.; Norman, N. C.; Schluter, E. *Angew. Chem., Int. Ed. Engl.* **1984**, *23*, 616.
(37) Burkey, D. J.; Hanusa, T. P. *Organometallics* **1995**, *14*, 11.
(38) Heeg, M. J.; Janiak, C.; Zuckerman, J. J. *J. Am. Chem. Soc.* **1984**, *106*, 4259.
(39) Overby, J. S.; Hanusa, T. P.; Young, V. G. *Inorg. Chem.* **1998**, *37*, 163.
(40) Evans, W. J.; Clark, R. D.; Forrestal, K. J.; Ziller, J. W. *Organometallics* **1999**, *18*, 2401.
(41) Atwood, J. L.; Hunter, W. E.; Cowley, A. H.; Jones, R. A.; Stewart, C. A. *J. Chem. Soc., Chem. Commun.* **1981**, 925.
(42) Jutzi, P.; Hielscher, B. *Organometallics* **1986**, *5*, 2511.
(43) Wrackmeyer, B.; Sebald, A.; Merwin, L. H. *Magn. Reson. Chem.* **1991**, *29*, 260.
(44) Kohl, F. X.; Dickbreder, R.; Jutzi, P.; Müller, G.; Huber, B. *Chem. Ber.* **1989**, *122*, 871.
(45) Wrackmeyer, B. *Annu. Rep. NMR Spectrosc.* **1985**, *15*, 73.
(46) Wrackmeyer, B.; Kupce, G.; Kehr, G.; Sebald, A. *Magn. Reson. Chem.* **1992**, *30*, 964.
(47) Janiak, C.; Schumann, H.; Stader, C.; Wrackmeyer, B.; Zuckerman, J. J. *Chem. Ber.* **1988**, *121*, 1745.
(48) Jutzi, P.; Dickbreder, R. J. *Organomet. Chem.* **1989**, *373*, 301.